Polymer 333 (2025) 128567

Contents lists available at ScienceDirect

Polymer

journal homepage: www.elsevier.com/locate/polymer

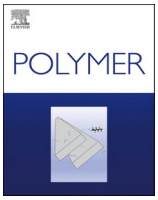

Electron beam modification of melt-spun polylactide fibers at elevated temperature

Yinglan Zhang [a,b], Michael Thomas Müller [a,*], Regine Boldt [a], Albena Lederer [a,c], Matthias Schwartzkopf [d], Norbert Smolka [a], Markus Stommel [a,b]

[a] Leibniz-Institut für Polymerforschung Dresden e.V., Hohe Straße 6, 01069, Dresden, Germany
[b] Institut für Werkstoffwissenschaft, Technische Universität Dresden, 01062, Dresden, Germany
[c] Department Chemistry and Polymer Science, Stellenbosch University, Private Bag X1, Matieland, 7602, South Africa
[d] Deutsches Elektronen-Synchrotron, Notkestr. 85, 22607, Hamburg, Germany

ARTICLE INFO

Keywords:
Polylactide
Additive-free
Electron beam modification
Orientation
Branching

ABSTRACT

Electron beam (EB) modification was carried out on the polylactide (PLA) fibers at the temperature both below and above the glass transition temperature (T_g) under nitrogen atmosphere. The irradiation at elevated temperature was performed by using a novel fiber stretching frame setup to protect fibers from shrinking, in which a permanent constant tension was loaded along fiber bundles to maintain their straightness throughout the irradiation. In contrast to irradiation at room temperature, where PLA predominantly undergoes chain scission, irradiation above T_g can introduce long chain branching (LCB) into the PLA matrix without the need of branching additives. The polymer chain orientation in the amorphous regions of drawn fibers is beneficial for achieving a higher yield of LCB. This improvement is attributed to the shortened intermolecular distance and the disentanglement in the amorphous domains which are caused by melt spinning and post-drawing. This is counteracted by the typically high crystallinity degrees in PLA fibers (measured by differential scanning calorimetry, 31.0 % – 41.2 % for neat fibers), due to the chain scission is mainly induced by EB in the rigid crystalline domains. The chain scission effect in the crystalline regions mitigates the branching effect in the amorphous regions on the material properties, such as tensile strength, even in irradiation above T_g. However, by reducing the PLA fiber crystallinity while applying temperatures above T_g, the amount of EB-induced LCB molecules was significantly increased. Moreover, the branched unit per PLA chain increases when a dose of 50 kGy is applied, as determined by analyzing the branching ratio g' using multi-detector size exclusion chromatography. In addition, the amount of branched unit also increases with the increasing irradiation dose. The tensile properties of fibers with varying drawing ratios were analyzed before and after irradiation. The resulting tensile properties are primarily determined by the draw ratio and appear to be barely affected by crystal orientation (examined using synchrotron X-ray scattering). However, the crystal orientation increases with higher irradiation doses (above T_g) and is likely driven by the interplay between chain scission and cold crystallization.

1. Introduction

Polylactide (PLA), as a biocompatible and biodegradable polymer, offers significant benefits for medical applications. For example, non-woven fabrics can be produced by PLA staple fibers to serve as scaffolds for bone tissue engineering. Although normally is the electro-spun PLA nanofibers used in scaffolds, some investigations on melt-spun PLA fibers have also been carried out, both woven and non-woven fabric are involved and the diameters of the fibers are in the range of 10 – 200 μm [1–5]. Moreover, it also can be used in many other fields, such as non-woven fabric using in oil absorption and oil/water separation [6]. Sometimes, in order to achieve a higher performance or meet some specific requirements, PLA fibers used in those fabrics need to be modified by adjusting the molecular structure. The commonly-used modification method for this aim is applying chemical additives. However, most chemical additives are toxic and not favorably for human health and the eco-system. This limits the wide application of PLA fibers, especially in the medical area. In order to overcome this issue, some

* Corresponding author.
E-mail address: Mueller-michael@ipfdd.de (M.T. Müller).

https://doi.org/10.1016/j.polymer.2025.128567
Received 30 January 2025; Received in revised form 13 May 2025; Accepted 18 May 2025
Available online 19 May 2025

solutions have been explored by researchers. Among them, achieving molecular structure alteration by electron beam (EB) irradiation is a promising method. Due to EB irradiation being a physical method, there will not be any additional chemical agents involved. Moreover, compared to chemical modification, it is more efficient. EB irradiation can mainly induce long-chain branching (LCB), cross-linking and chain scission. The crystallization behavior of the material may also be changed by irradiation, due to the molecular structure alteration. In some cases, the change in crystallization behavior can improve the properties of the polymer. However, even though EB irradiation can easily enhance properties by modifying the molecular structure of many polymers, there is an issue in the case of PLA. This is because PLA is a kind of irradiation-degraded polymer. During EB irradiation, high energy electrons will induce LCB, cross-linking and chain scission into polymer material at the same time, these three reactions compete with each other. In the case of PLA irradiation, the chain scission normally is the dominant reaction, branching and crosslinking can only be induced by adding chain extender agents into PLA [7–15]. For instance, the trimethylolpropane triacrylate (TMPTA) and triallyl isocyanurate (TAIC) are the common-used chain extender agents [10–12,16–18]. LCB and cross-linking can enhance the material property, such as durability, however, if there is too much chain scission, the degradation effect will overlay the LCB and cross-linking effect, resulting in damage to the material and reducing mechanical properties of PLA.

To solve this issue, efforts have been made by many researchers, and a breakthrough has been reported in 2019 [19]. An obvious weight-average molecular weight (M_w) increase and cross-linked gel have been found in the irradiated PLA, which is irradiated by EB without using any chemical chain extenders. It is reported that the key point to achieve M_w increase in additive-free PLA is using an irradiation temperature above the glass transition temperature ($T_g \sim 60$ °C) of PLA. Subsequently, more evidence of LCB and cross-linking in PLA that irradiated at $T > T_g$ has been found [20,43]. However, these researches only deal with compression-molded non-oriented PLA bulks, where no fiber shaping is involved. For the PLA fiber irradiation, only gamma or EB irradiation performed at room temperature has been reported [13,21]. The PLA fibers produced by melt spinning have oriented crystalline structures (lamellae), oriented amorphous chains (mesophases [22,23]) and random-entangled amorphous chains in the case of semi-crystalline fibers and oriented amorphous chains with random-entangled amorphous chains in the case of amorphous fibers. The oriented structures, which includes oriented chains in both crystalline and amorphous areas, could be irreversible eliminated when the mobility of chain segments was improved by thermal heating [24]. Therefore, the biggest issue that hinders researchers applying a $T > T_g$ on fiber irradiation is the uncontrollable shrinkage of fiber at that temperature range. The orientation structure in the fibers will be lost with the temperature increasing to such elevated temperatures, thereby losing their important mechanical properties. When start heating from room temperature, a slight shrinkage could take place firstly in the range up to T_g caused by the moisture, if the fibers are not dried sufficiently. When the temperature is around the T_g, the entropy shrinkage occurs, i.e. the oriented amorphous chain segments will relax rapidly, leading to a distinct shrinkage. By further increasing the temperature up to the onset of melting, the cold crystallization could occur in fibers during thermal treatment, especially in fibers with high draw ratio, also contributing to shrinkage via chains aligning into the more compact crystalline structure. Accordingly, no publication has involved an elevated temperature in PLA fiber irradiation so far. However, in the stretching-induced orientation structure, the chains were disentangled and the intermolecular distance could be decreased. The decreasing distance can increase the possibility of radical chains moving close to each other for branching and crosslinking reactions. Some researchers found increasing the compression pressure that applied during the polymer irradiation can obviously enhance the irradiation-induced crosslinking in some polymers, such as butadiene rubber and styrene-butadiene rubber, even though it is not for polymers like ethylenepropylene rubber and poly(tetrafluoroethylene-co-propylene) [25,26]. There are some attempt on protecting the orientation structure from shrinkage among the scientists working in instrumental analysis in differential scanning calorimetry [27]. They constraining the fiber at high temperature by winding fibers on the thin metal plate and tie or stick the fibers ends to fix the fibers. On the other hand, the EB irradiation is also a common method for sterilization of PLA that used in medical (e.g. implantable materials) and food packing applications [28,29]. This is another importance to investigate the EB irradiation effect on PLA fibers.

In this study, the elevated temperature irradiation was applied to PLA fibers. The thermal-induced shrinkage of fiber was overcome by applying a novel processing method to keep the fiber straight during irradiation, i.e. added a permanently constant tension along the fiber bundle. The effect of the tension on the irradiation modification was discussed based on the characterization of crystal orientation, as the crystal orientation can be seen as an indicator of the tension condition in fibers. The irradiation effect on the industrial commonly-used PLA fibers, which had undergone both crystallization and stretching, were discussed. To separate the effect of stretching from crystallization, the EB irradiation modification on the amorphous fibers that almost without crystallization was investigated. Furthermore, to separate the effect of stretched (oriented) amorphous chain from non-stretched (non-oriented), the comparison between the EB-irradiated amorphous fiber (with oriented amorphous chains) and bulk (with non-oriented amorphous chains) was carried out. The chain scission and branching were determined by multi-detector size exclusion chromatography (SEC), the crystal orientation of semi-crystallized fibers was examined using synchrotron X-ray (wide-angle X-ray scattering, WAXS), the crystallinity was evaluated by differential scanning calorimetry (DSC), and the mechanical properties of fibers was measured by tensile test.

2. Experimental section

2.1. Materials

PLA granules with the grade 6202D were purchased from NatureWorks LLC, USA. Tetrahydrofuran (THF) was stabilized with 0.025 % butylated hydroxytoluene (BHT).

2.2. Fiber and bulk PLA preparation

Granules were dried at 40 °C, 16 h under vacuum before all spinning. The granules stored and fall into the spinning machine under nitrogen. The spinning was conducted at room conditions.

Crystallized fibers (commercial commonly-used type) were produced at Leibniz Institute of Polymer Research Dresden (IPF Dresden) by melt spinning using a self-built extrusion-spinning equipment. The throughput is 25 g min^{-1}, temperature of the melt finally reaches to 241 °C, extruder zone temperatures are 180, 210, 228 and the temperatures of spinning head and die are both 230 °C, take-up velocity is 2475 m·min^{-1}, winding velocity is 2538 m·min^{-1}, godet (which used to change the fiber transfer direction) velocity is 2500 m·min^{-1}, the capillary die has 3 holes, the hole has a diameter (D) of 0.5 mm and the length (L) to D ratio (L/D) of 2. After spinning, the multi-filament (yarn) contained 3 single fibers was obtained. In the following offline drawing process, the multi-filament that contains 6 single fibers was obtained by combining two multi-filaments that contains 3 single fibers in each of them at drawing temperature, around 80 °C. Neat fibers with four different draw ratio (DR), 1.0, 1.2, 1.4 and 1.6, were produced by the drawing process, which was named as DR1.0-neat, DR1.2-neat, DR1.4-neat and DR1.6-neat. The fineness of the multi-filament yarn DR1.0-neat, DR1.2-neat, DR1.4-neat and DR1.6-neat are around 200, 167, 143 and 125 dtex, respectively.

Amorphous fibers were produced by a self-built piston-type melt spinning device (IPF Dresden). The throughput is around 1 g·min^{-1} and the temperature of melt spinning is 230 °C. As the device has a very small barrel (around 10 cm^3), this is the only settable temperature. The

diameter (D) of the one-hole capillary is 0.3 mm and the L/D of the capillary is 2. After the melt flow squeezed out from the die, it was collected by one roller directly using winding velocities of (V) 50, 75, 100 and 150 m·min^{-1}. Then they are ready to be used in fiber bundle preparation, which is a manual process the same as what was applied on crystallized fibers. No drawing process was applied after or during spinning. After spinning, the single fibers (i.e. monofilaments) were manually combined to multi-filaments that contains 6 single fibers for fineness determination. The fineness of the neat yarn of the amorphous multi-filament that contains 6 single fibers with the winding velocities of 50 (V50-neat), 75 (V75-neat), 100 (V100-neat) and 150 (V150-neat) m·min^{-1} are around 955, 629, 489 and 324 dtex, respectively.

The non-orientated bulk PLA (amorphous) was prepared by vacuum compression molding. The detailed parameters are shown in our previous work (the sample '0-neat', which is prepared without holding at crystallization temperature 110 °C during cooling) [20].

2.3. EB irradiation method

A novel fiber stretching frame setup is utilized to maintain the fibers straight during the irradiation process when the elevated temperature T > T_g is applied, as demonstrated in Fig. 1(a) and (b). PLA bundles composed of 150 single fibers were used in irradiation. The bundle was fixed by taping one end to a metal frame and adding a load to the other end. The sensor tests the temperature inside the bundle. The load helps to maintain a generally constant fiber length during elevated temperature irradiation, ensuring that the chain and crystalline orientations within the fibers were not destroyed despite the heating. The loading weights are shown in Table 1. The criteria used for the load selection was established on an empirical basis to ensure that the fibers remain straight during irradiation at elevated temperature (T > T_g) and to prevent them from diameter change. The load 10.6 g (0.1 N) works well in the case of crystallized fibers with lower DR (1.0 – 1.4) and amorphous fibers, while it cannot prevent the fibers with high DR (1.6) from shrinking. Accordingly, the load was increased to 51.2 g (0.5 N) for DR1.6. This may be due to the highly oriented amorphous structures in high DR (1.6) fibers leads to greater entropy shrinkage and additional contraction from cold crystallization. At 80 °C, in contrast to the significant shrinkage observed in the fiber bundle with the free ends Fig. 2 (a), the fiber bundle with the fiber stretching frame setup described above remained straight Fig. 2(b). For irradiation performing at 25 °C (room temperature) and in the case of non-oriented amorphous bulk PLA, no stretching frame setup was used, as it is unnecessary.

Prior to irradiation, the samples were dried in a vacuum oven (0 mbar) at approximately 40 °C for 24 h, and the electron accelerator ELV-2 (Budker Institute of Nuclear Physics in Novosibirsk, Russia) was employed for all irradiations. A closed chamber was used to achieve the nitrogen atmosphere during irradiation. The temperature was heated up to 80 °C and kept for 5 min under a vacuum after closing the chamber, in order to remove the moisture and oxygen. After that, the temperature was set up to the target irradiation temperatures and irradiation was performed under a nitrogen atmosphere. Samples were taken out of the irradiation chamber after they cooled down to room temperature. Irradiation doses applied in this study are 0, 25, 50 and 250 kGy. The energy and current of the EB are 1.5 MeV and 4 mA, respectively, during the whole irradiation. The 25 °C, 75 °C and 80 °C are used as irradiation temperatures. The thickness of our fiber bundle is in the range of 1 – 2 mm (for the crystallized fiber is close to 1 mm and amorphous fiber is close to 2 mm) and the non-orientated bulk PLA is 2 mm. The electron beam can penetrate through the whole samples in all the case in this study. However, it needs to be noted that due to the irradiation modification here is induced by accelerated electrons, there is a dose distribution due to the electron back scattering effect in the irradiated polymer material (i.e. the electron from scattering encounter each other so that has a maximum energy at a certain position). The error of irradiation dose is 10 % – 30 %.

Table 1
Loading weights used in the stretching frame setup in elevated temperature irradiation.

Loading Weights	Crystallized Fiber	Amorphous Fiber
	Draw Ratio (DR)	Winding Velocity (V) [m·min^{-1}]
10.6 g (i.e. 0.1 N)	1.0	50
	1.2	75
	1.4	100
	/	150
51.2 g (i.e. 0.5 N)	1.6	/

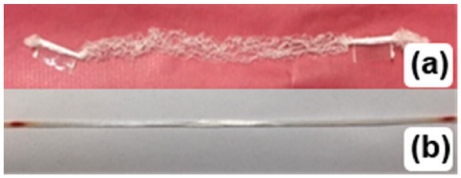

Fig. 2. (a) Unloaded and (b) weight-loaded (using fiber stretching frame setup) PLA fiber bundles of 150 single fibers after thermal treatment above T_g (80 °C).

3. Characterization

3.1. DSC

The fiber bundles were cut into small pieces, mixed and dried in vacuum oven at 40 °C (around 0 mbar) for 24 h before test. The fibers are able to shrink freely during the measurement. The differential scanning calorimeter DSC Q2000 (for crystallized fibers) and Q1000 (for amorphous fibers) from TA Instruments were applied. Approximately 6 mg of samples were used in each measurement. A heating-cooling-

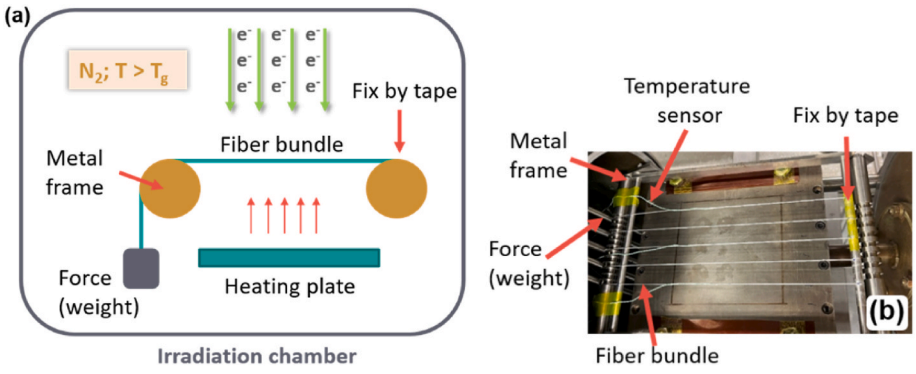

Fig. 1. (a) Schematics and (b) the picture of experimental setup of fiber irradiation with fiber stretching frame.

heating mode was applied. The 1st heating scan was performed from room temperature or −80 °C to 220 °C or 250 °C and hold at this temperature for 1 – 3 min to erase the thermomechanical history. Then, the temperature was cooled down to −80 °C. After that, the 2nd heating scan started from −80 °C to 220 °C or 250 °C. All tests were carried out under N_2 atmosphere with heating and cooling rates of 10 K min^{-1}. Crystallinity (X_c) was calculated by Equation (1).

$$X_c = \frac{(\Delta H_m - \Delta H_{cc})}{\Delta H_m^0} \times 100\ \% \quad (1)$$

where ΔH_m and ΔH_{cc} are the melting and cold crystallization enthalpy, respectively. ΔH_m^0 is the melting enthalpy of pure PLA with 100 % crystallinity, which is 93.7 J g^{-1} [30].

3.2. Diameter

The diameter is determined using a light microscope (Keyence VHX 2000). The fibers are embedded in an epoxy resin and cured, and then ground and polished using a grinder device QAtm (Opal 250 A1-Eco).

3.3. WAXS

In order to study the orientation of the crystalline fibers, synchrotron X-ray measurements were performed at the P03/MiNaXS beamline of the PETRA III Synchrotron (DESY, Hamburg, Germany) with a beam size of 22 × 30 μm^2 and a wavelength of 0.1044 nm [31]. Single fibers were scanned perpendicular to the flow direction with an increment of 0.01 mm. The travel path of the focus is longer than the diameter, i.e. the focus starts moving from the position outside the fiber, then moves onto the fiber, and finally moves to the other side outside the fiber. The images were acquired using a LAMBDA 9 M detector (X-Spectrum, 55 μm pixel size). For evaluation of orientation, the patterns were integrated radial using the DPDAK software (version 1.59). The signal of the crystal plane [2 0 0], i.e. the peak at 2θ ~ 16.7° [20], was used in the comparison of crystal orientation. The signal which has the maximum peak height was selected from multiple azimuthal profiles for the comparison. A schematic of the measurement is shown in Fig. 3.

3.4. SEC

The absolute molar mass and branching analysis were examined using multi-detector SEC. For this purpose, SEC was coupled to multi-angle light scattering detector (MALS), refractive-index detector (RI) and intrinsic viscosity detector (IV), namely SEC-MALS-IV. The absolute molar mass, which is independent of elution time or column calibration, was determined by a MALS detector combined with a RI detector. Two high-performance liquid chromatography (HPLC) columns (PLgel 5 μm, 300 × 7.5 mm, MIXED-C column, Agilent Technologies) were used. The HPLC pump (1100 series from Agilent Technologies, US) was coupled to the MALS detector DAWN HELEOS, the viscometer ViscoStar and the RI detector Optilab T-rEX are from Wyatt Technology. A temperature of 25 °C and a flow rate of 1.0 mL min^{-1} were applied in the measurements. The data analysis was done on the ASTRA 7.3.2 software (Wyatt Technology). A drying for samples was done in vacuum at around 40 °C (0 mbar) for 24 h before measurements. THF was used as the solvent, samples were dissolved in it 2 h at room temperature and then around 3 h at 55 °C, making the solution with concentration of around 3.5–4 mg ml^{-1}. After cooling down to room temperature, the solutions were filtered by a 0.2 μm hydrophobic polytetrafluoroethylene (PTFE) filter and injected into the instrument. Butylated hydroxytoluene (BHT) with an amount of 0.025 % was used to stabilize the solvent THF. Each sample has been measured in triplicate to ensure reproducibility, the results presented in this paper are the average value or plot of the measurement results. The non-irradiated (0 kGy) samples, which did not receive EB treatment but underwent all other treatments same as the irradiated samples, acted as linear references in the LCB analysis. The insoluble part with an amount of around 0.30 wt% in the case of crystallized fibers was ignored, since the very low percentage.

3.5. Tensile test

A tensile test device of Zwick/Roell Z0.5 (Zwick/Roell Company,

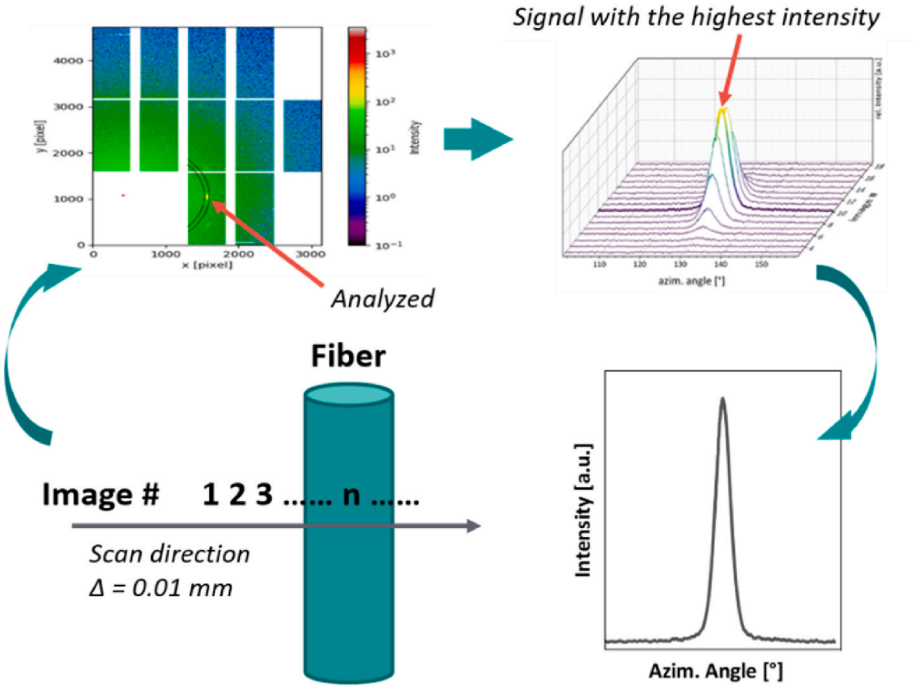

Fig. 3. Scheme of the fiber and the scan direction of X-ray measurement is perpendicular to the fiber. Multiple WAXS patterns are obtained (here is one for an example) and the integrated azimuthal angle is shown as black dotted ring segments. Resulting azimuthal profiles of WAXS patterns along the fiber diameter. Signal with the highest intensity is selected.

Germany) was used to test PLA fibers at room temperature. The distance between the clamps at the start position is 50 mm. The crosshead moves with a speed of 100 mm·min^{-1} for the test of crystallized fibers, while 10 mm·min^{-1} in the case of amorphous fibers since they are very brittle and break easily when a high test speed was applied. Fiber bundles containing 6 single fibers were used for testing. They were separated from the bundle composing of 150 single fibers, and were taped together at the fiber ends to make a multi-filament for test. The fineness-related maximum tensile strength, f_H (max), which is the force per fineness united in cN·tex^{-1}, was used here. The crystallized fibers revealed a strain hardening after the yield point, so the f_H (max) is also the strength at the break. The amorphous fibers did not undergo strain hardening since the brittleness, thereby the f_H (max) for those fibers is the maximum strength before breaking. It needs to be noted that due to the brittleness of the amorphous fibers, they break at the fiber ends but not at the middle. It may be because the clamps applied additional stressing forces onto the fiber ends. The fineness in dtex was determined by analytical balance, in which a specific length of fiber was measured. Each kind of fiber was tested more than three times, and the results presented in this paper are the average values with the standard deviations as the error bars. The fineness of neat crystallized fibers was used in the calculation of their tensile properties, as they were basically not changed by thermal treatment. However, because the fineness of amorphous fibers was decreased by 3 – 9 % (caused by the stretching frame method used in this study, original fineness shown in section 2.2), the fineness after the thermal treatment was used for more accurate results in tensile property calculation, which are 869, 607, 450 and 299 dtex, for V50, V75, V100 and V150 fiber, respectively.

4. Results and discussion

4.1. Irradiation on industrial commonly-used PLA fibers

4.1.1. Crystallinity and diameter

The industrial commonly-used PLA fibers that with crystalline structures was irradiated firstly. Based on the literature, the optimal irradiation temperature for increasing weight-average molecular weight (M_W) is 80 °C, because it allows an adequate polymer chain mobility to facilitate intermolecular backbone radical recombination [19]. However, crystalline PLA fibers begin to undergo cold crystallization right after surpassing T_g, as shown in Fig. 4. This cold crystallization increases crystallinity during irradiation at temperatures above T_g. Previous research suggests that high crystallinity hinders the M_W increase in the EB irradiation modification of PLA [20]. Accordingly, the thermally induced changes in crystallinity were evaluated first, prior to assessing the effects of irradiation. For this purpose, neat fibers were subjected to the same thermal treatment as the irradiated fibers have undergone in irradiation (at 80 °C). The crystallinities of the neat fibers (25 °C, 0 kGy) with the draw ratio DR1.0, DR1.2, DR1.4 and DR1.6 were increased by 15.3, 9.2, 6.9 and 6.7 percentage points, respectively, after the thermal treatment (80 °C, 0 kGy), as shown in Fig. 5. This suggests that the fiber crystallinity at the moment of EB entry at 80 °C is higher than the crystallinity of neat fibers. On the other hand, double melting peaks appeared during the first DSC heating scan, becoming more pronounced as the DR increased, as shown in Fig. 4. It implies that unlike low DR fibers, the fibers with higher DR contain two distinct crystal types, α and α'. The newly generated peaks appearing at lower temperature correspond to α′ crystals, which are less densely packed than α crystals. The presence of α′ crystals and lower exothermal enthalpy of cold crystallization suggest that the drawing process has reduced the intermolecular distance and induced more crystallization in the fiber. This phenomenon becomes more pronounced in thermally treated fibers, as evidenced by the increased percentage of α′ crystals (see supplementary SFig. 1). This suggests that the thermal treatment in combination with the stretching frame setup results in an additional intermolecular distance reduction. During 80 °C irradiation, fiber shrinkage was effectively prevented by using the stretching frame setup, and thermal treatment generally did not change the diameter of the crystallized PLA fibers. The diameters with fineness of neat and thermally treated fibers are presented in Table 2, with examples of microscope images provided in supplementary SFig. 2 and SFig. 3.

4.1.2. Molecular structure alteration

The influence of temperature on the EB-induced molecular structure alteration in PLA fibers was investigated. Neat crystallized PLA fibers were exposed to irradiation at 25 °C ($T < T_g$) or 80 °C ($T > T_g$), T_g is around 61 °C according to Fig. 4. By applying a multi-detector SEC, the relative differential molar mass distributions (MMD) were obtained. There is no obvious difference in irradiation effect among the fibers with different DR, the comparison of MMD plots between all DRs are shown in supplementary SFig. 5, therefore, only the fiber with DR1.0 is discussed here as an example. According to Fig. 6, the MMD of non-irradiated crystallized fibers (0 kGy), which means other conditions were identical to those of the irradiated samples but no irradiation dose was applied, are almost the same whether the irradiation was conducted at 25 °C or 80 °C. It suggests that the thermal treatment alone does not

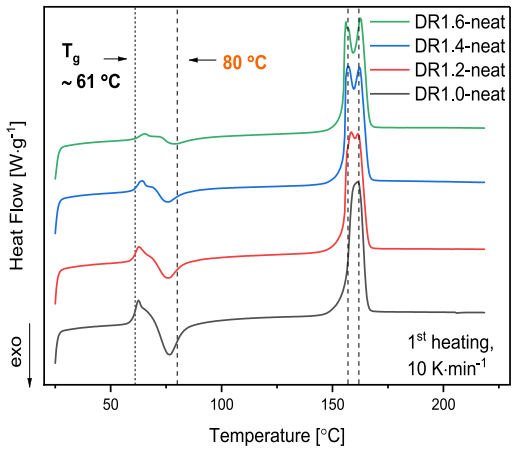

Fig. 4. DSC thermograms of neat crystallized fibers with DR 1.0 to 1.6, in which T_g is around 61 °C and irradiation temperature is 80 °C.

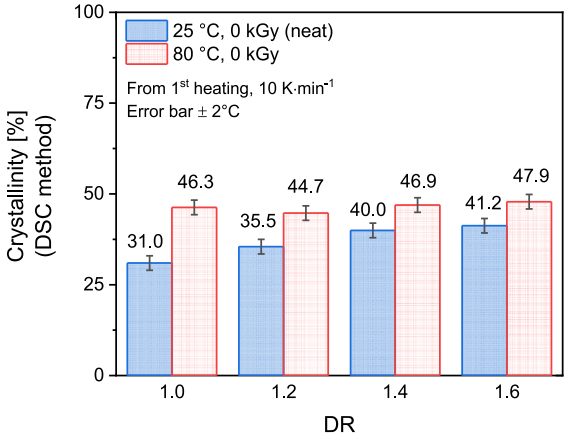

Fig. 5. Crystallinity determined by DSC method for neat (25 °C) and thermally-treated (80 °C) fibers with DR 1.0 to 1.6.

Table 2
Diameters and fineness of neat (25 °C) and thermally-treated (80 °C) crystallized PLA fibers with DR 1.0 to 1.6.

DR	Diameter* [μm]		Fineness [dtex]	
	Neat (25 °C, 0 kGy)	80 °C, 0 kGy	Neat (25 °C, 0 kGy)	80 °C, 0 kGy
1.0	59 ± 2	61 ± 3	200	196
1.2	57 ± 4	56 ± 6	167	161
1.4	49 ± 2	51 ± 2	143	137
1.6	47 ± 1	48 ± 1	125	120

*Average values ± standard deviations.

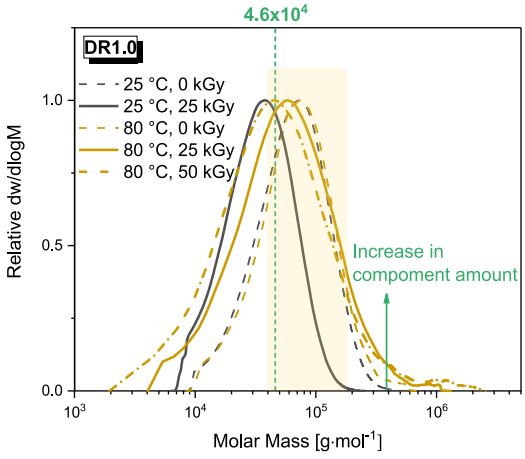

Fig. 6. Relative molar mass distribution of non-irradiated (0 kGy) and irradiated (25 and 50 kGy) PLA fibers with DR1.0 at 25 and 80 °C.

result in significant chain scission. In contrast, the MMD of fibers receiving 25 kGy irradiation shifts towards lower molar mass region compared to non-irradiated fibers, in the both cases of irradiation performed at 25 °C and 80 °C, which implies the occurrence of the irradiation-induced chain scission. However, there are differences between the case of 25 °C and 80 °C. The MMD of 80 °C irradiation is broader, shows a slighter shift from non-irradiated fibers than the 25 °C case, and also includes an increased amount of higher molar mass components. The dispersity index M_w / M_n is an indicator of the broadness of the MMD and can be found in Table 3. By comparing the irradiated fiber with the non-irradiated, it also can be found when irradiated with a dose of 25 kGy at 25 °C, the spectrum shifts to a lower molar mass range and the dispersity index almost is not changed. However, it is noticeably increased for fibers irradiated at 80 °C with the same dose, which is a result of the increased amount of higher molar mass components. The number- (M_n) and weight- (M_w) average molar masses are also listed in Table 3, and chromatograms are in supplementary S.Figs.6-22. In addition, the full peak widths at half the maximum peak value (FWHM) are shown in supplementary in SFig. 23. Moreover, compared to fibers irradiated at 25 °C, the fibers irradiated at 80 °C reveal a lower relative MMD in the low molar mass region (around 1×10^4 to 4.6×10^4 g·mol^{-1}) and a higher relative MMD in the high molar mass region (above 4.6×10^4 g·mol^{-1}). This suggests that an irradiation temperature of 80 °C leads to larger amount of high molar mass components than 25 °C. On the other hand, when the irradiation dose is increased to 50 kGy with 80 °C, the lower molar mass components are increased in amount but only very minor increase for higher molar mass components, compared to the 25 kGy case. It suggests that the increasing dose is beneficial for chain scission.

To explore the underlying reason of the phenomena above, a branching analysis was conducted. The traditional branching analysis involves assessing the difference in macromolecular volume between branched macromolecular chains and their linear equivalents [32]. Typically, the contraction factor g, which is calculated from the radii of gyration of the branched and linear polymers, is used for this purpose. However, determining the radii of gyration using MALS is only feasible for angle-dependent scattering, which occurs in macromolecules larger than 1/20 of the used laser wavelength (650 nm). The PLA samples in this study did not reach that size, thereby the branching ratio g' was used as an alternative, which depends on the polymer size [33]. The size reduction in this case is represented by the ratio of the intrinsic viscosities of the branched and linear polymers [34,35]. The determination of g' is based on measurements from a viscosity detector coupled to SEC and is calculated using Equation (2), where [η] is the intrinsic viscosity, and the subscript M indicates the calculation is performed at the same molar masses for the linear and the branched structure [36]. As branched molecular chains are more compact than the linear chains at the same molar mass, the branching can be evaluated based on the changing of g'. The g' decreases with the branching occurs, that is, the lower the g' the more the branch units. The molar mass dependence of g'

Table 3
M_n, M_w and M_w/M_n of non-irradiated (0 kGy) and irradiated (25 kGy or 50 kGy) fibers with different draw ratio (DR).

DR	Irradiation Temperature [°C]	Irradiation Dose [kGy]	M_n* [kg·mol^{-1}]	M_w* [kg·mol^{-1}]	M_w/M_n
1.0	25	0	48.9 ± 0.1	76.2 ± 0.3	1.6
1.0	25	25	27.9 ± 1.0	40.7 ± 0.4	1.5
1.2	25	0	49.1 ± 0.4	77.3 ± 0.1	1.6
1.2	25	25	24.6 ± 0.1	40.4 ± 0.3	1.6
1.4	25	0	50.7 ± 0.3	78.3 ± 0.5	1.5
1.4	25	25	24.8 ± 0.1	40.5 ± 0.3	1.6
1.6	25	0	49.7 ± 0.7	77.8 ± 0.6	1.6
1.6	25	25	26.1 ± 0.7	43.7 ± 0.7	1.7
1.0	80	0	52.4 ± 1.8	85.6 ± 2.4	1.6
1.0	80	25	34.9 ± 1.0	82.6 ± 2.4	2.4
1.0	80	50	24.7 ± 0.5	82.7 ± 10.4	3.4
1.2	80	0	49.9 ± 1.1	78.9 ± 0.8	1.6
1.2	80	25	33.3 ± 0.7	73.1 ± 1.1	2.2
1.4	80	0	49.4 ± 2.0	79.4 ± 1.7	1.6
1.4	80	25	33.1 ± 2.5	73.8 ± 0.7	2.2
1.6	80	0	51.4 ± 3.6	78.8 ± 1.6	1.5
1.6	80	25	34.5 ± 2.1	73.9 ± 2.1	2.1

*Average value ± standard deviation

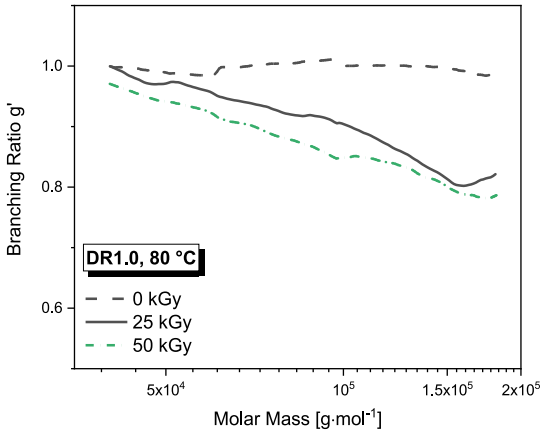

Fig. 7. g' plot of non-irradiated (80 °C, 0 kGy) and irradiated (80 °C, 25 or 50 kGy) PLA fibers with DR1.0.

of fibers irradiated at 80 °C were analyzed, as shown in Fig. 7. The molar mass range from approximately 4×10^4 to 1.8×10^5 g·mol^{-1} was selected, which is in the overlap of non-irradiated (80 °C, 0 kGy) and irradiated (80 °C, 25 kGy) PLA fibers, highlighted range in Fig. 6. No obvious difference was found among the fibers with different DR, the g' for other DRs are shown in supplementary SFig. 24, thereby only DR1.0 is discussed here as an example. It was observed that the g' values for non-irradiated fiber are around 1.0 in this region, which is typical for linear polymers. For 25 kGy irradiated fibers, g' decreases with increasing molar mass, indicating greater compactness and suggesting the occurrence of branching. This implies that branching forms in fibers during irradiation at 80 °C with 25 kGy. It explains why the fibers irradiated at 80 °C with 25 kGy have a higher amount of high molar mass components than those irradiated at 25 °C with the same dose (Fig. 6), that is, the EB induces more branched molecules at that elevated temperature. Additionally, the effect of irradiation dose was examined, and the g' slightly decreased when the dose was increased to 50 kGy, suggesting that more branch units are induced in the polymer chain by increasing the irradiation dose.

$$g' = \left(\frac{[\eta]_{branched}}{[\eta]_{linear}} \right)_M \tag{2}$$

In polymer irradiation, EB exposure generates radicals along the polymer backbone in PLA fibers by abstracting hydrogen atoms. These radicals can then recombine with other radical chains forming branches. To achieve recombination, two radicals, which possess thermodynamically excited unpaired electrons, must be sufficiently close for their electron orbitals to overlap, which allows the system to return to a thermodynamically ground state. When irradiation is conducted at the temperature below T_g, the polymer chains exhibit limited mobility in both the crystalline and amorphous regions, resulting in only a minimal amount of EB-induced branching. In contrast, when an irradiation temperature above T_g is applied, more chains in the amorphous region gain better mobility, leading to greater opportunities for intermolecular radical recombination. Thus, conducting irradiation at 80 °C promotes more extensive branching induction, as evidenced by the increased presence of high molar mass chains compared to fibers irradiated at 25 °C with the same dose. Additionally, very low amounts of gel content were observed in PLA fibers irradiated at 80 °C with a high dose of 250 kGy, below 12 %, which indicates that a small degree of cross-linking occurred, as noted in supplementary STable 1. On the other hand, it was observed that EB irradiation only resulted in a minimal number of components exceeding the highest molar mass of non-irradiated fibers,

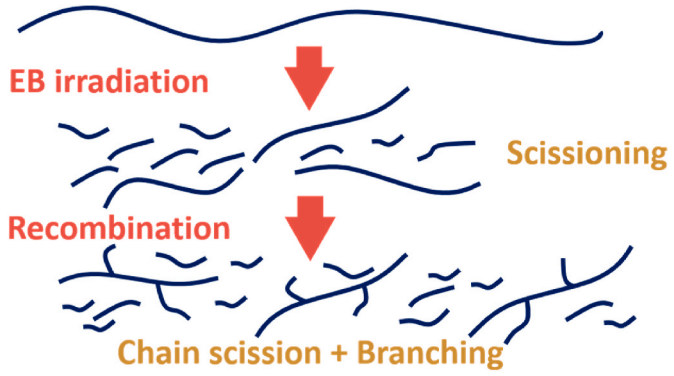

Fig. 8. Schematic of reactions during irradiation.

even at the temperature above T_g. This can be attributed to the high crystallinity level (approximately 45 % for all DR) of fibers treated at 80 °C as well as the EB-induced chain scission reactions compete with the EB-induced branching. Additionally, the number of highly mobile chains in the amorphous regions is insufficient to produce a substantial quantity of branched polymer chains. Consequently, the majority of polymer backbone radicals experience main chain scission, resulting in shorter PLA chains. Following this, hydrogen atom abstraction occurs along these shorter chains, generating radical chains. These shorter polymer radical chains then recombine with other mobile chains, forming branches, as illustrated in Fig. 8. As a result, although branching takes place, most of the branched chains do not possess a higher molar mass than the original linear chains. Additionally, increasing the applied irradiation dose is found not an effective strategy for promoting branching on high molar mass molecules in highly crystallized PLA fibers. This is evident when the irradiation dose is doubled from 25 kGy to 50 kGy, leading to a significant rise in low molar mass components but only a slight increase in high molar mass components, as it was shown in Fig. 6. This indicates that a higher irradiation dose results in more chain scission than branching.

It needs to be noted that although no obvious difference was found in our case, it does not rule out DR as a potential factor in molecular structure modification in all the cases. For room temperature irradiation, it could attributed to the all chains do not have enough mobility for reactions that can increase molar mass, e.g. branching. For the elevated temperature irradiation, it may be attributed to the crystallinity increases to a similar level after cold crystallization in our case, as shown in Fig. 5. Because in our case a special irradiation method was used, in which the fiber stretching frame setup was applied, there is also a possibility that the DR effect was eliminated by this method. Multiple factors could overlap, such as crystallinity, chain orientation in the amorphous regions, and the applied load force on fibers during irradiation.

4.1.3. *Crystal orientation*

In this study, a permanently constant load was applied onto the fiber during irradiation to keep the fiber straight at elevated temperature, as was mentioned in section 2.3. However, as the multiple reactions were induced inside the PLA material during the elevated temperature irradiation, such as the cold crystallization and molecular structure alteration, the interaction between the constant force and the material is quite complex during the irradiation. To figure out the effect of the tension on the irradiation modification, the synchrotron X-ray scattering was performed to characterize the crystal orientation, as the crystal orientation can be seen as an indicator of the tension condition in fibers. The relative orientation parameters (O_{rel}) calculated by FWHM of relative intensity ($O_{rel} = 1$ means 100 % orientated, $O_{rel} = 0$ means non-oriented) show an instinct increase after thermal treatment but less change after receiving 25 kGy and 250 kGy irradiation, Table 4. This

Table 4
Relative orientation (O_{rel})[a)] and maximum relative intensity determined by WAXS of the crystallized PLA neat fibers and fibers irradiated at 80 °C with a dose of 0 – 250 kGy.

DR	Neat		0 kGy		25 kGy		250 kGy	
	O_{rel}	Max. rel. Intensity	O_{rel}	Max. rel. Intensity	O_{rel}	Max. rel. Intensity	O_{rel}	Max. rel. Intensity
1.0	0.904	5	0.957	51	0.957	54	0.956	61
1.2	0.935	12	0.967	56	0.955	53	0.968	66
1.4	0.958	38	0.971	56	0.971	70	0.970	68
1.6	0.959	45	0.967	47	0.973	67	0.974	79

[a)] $O_{rel} = (180° - FWHM)/180°$

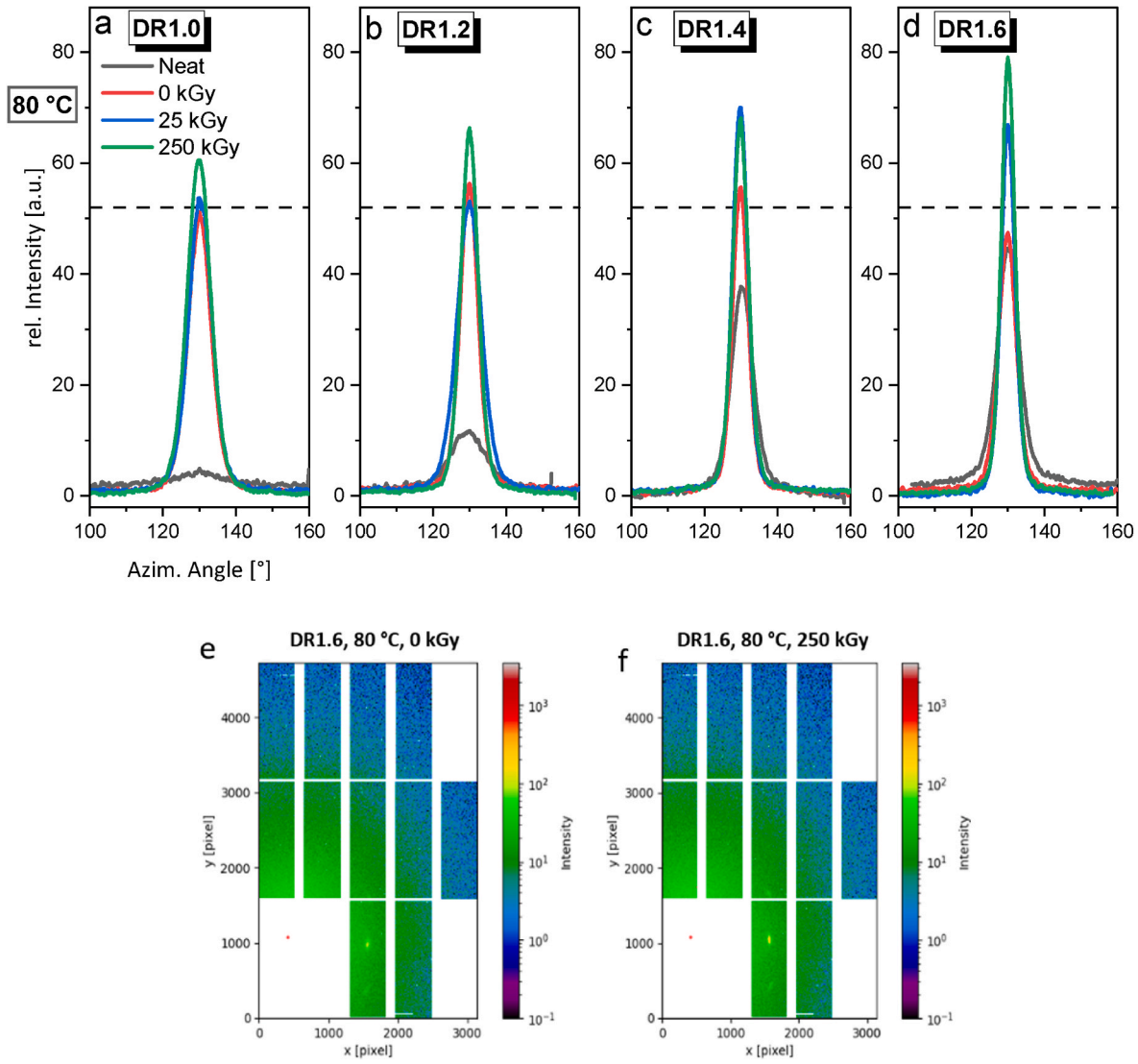

Fig. 9. Wide-angle X-ray scattering results of neat, thermal-treated and irradiated (25 and 250 kGy) crystallized PLA fibers with draw ratio DR (a) 1.0, (b) 1.2, (c) 1.4 and (d) 1.6, as well as the 2D patterns of (e) the thermal-treated non-irradiated and (f) 250 kGy irradiated fiber with DR 1.6.

suggests thermal treatment is the main factor that influences the crystal orientation. On the other hand, the signal intensity of neat fibers (without thermal treatment) rose with increasing DR, indicating the higher the DR, the higher the crystal orientation of the neat fibers is, Fig. 9(a)–(d). However, after conducting thermal treatment at 80 °C with the fiber stretching frame (0 kGy, under stress load), the signal intensities of the fibers surpassed those of the neat counterparts, indicating an increase in crystal orientation. Among the different DRs, the fiber with DR1.6 showed only a slight increase in crystal orientation, whereas the increases for fibers with DR1.0, DR1.2, and DR1.4 were more pronounced. Consequently, the crystal orientation of thermal-treated fibers with the four different DRs becomes similar after thermal treatment. The trend of crystal orientation change is in accordance with the trend of crystallinity change (Fig. 5) that observed after thermal treatment. Thus, the increase of the signal intensity can be caused by the increasing crystallinity, as signal intensity corresponds to the number of crystals aligned along the axial direction of the fiber. Regarding one end of fiber bundle was added a load during the whole thermal treatment (as described in experiment section 2.3), there is an additional stretching force along the axial direction of fiber, which can lead thermal-induced

crystallization to occur along the fiber direction. Therefore, the increase in signal intensity could be attributed to the newly formed crystalline structures that aligned along the axial direction of fiber. On the other hand, after conducting an irradiation at 80 °C with 25 kGy, no significant changes were found in the signal intensity for fibers with DR1.0 and DR1.2, compared to their thermally treated counterparts, Fig. 9(a) and (b). This suggests that the 25 kGy EB irradiation did not significantly increase the number of crystals aligned along the axial direction in these fibers. However, for fibers with DR1.4 and DR1.6, the intensity increased after 25 kGy irradiation, indicating that more crystals are aligned along the axial direction, Fig. 9(c) and (d). One possible explanation for this is the combined effect of EB-induced chain scission and thermal-induced crystallization occurring simultaneously during the irradiation. As shown by the SEC results, Fig. 6, chain scission occurred in fibers exposed to a 25 kGy dose irradiation, resulting in the formation of shorter chains. These shorter chains exhibit less entanglement, which reduces the internal resistance of the fiber to the stress applied along the fiber (stretching frame setup). Since the stress load, which remains constant in the whole irradiation, will act as an additional stretching force and transfer to the crystals, an enhancement of crystal orientation will occur with the decreasing resistance in fiber to the stress, i.e. the realignment of the pre-existing crystal could occur. This additional stretching also could induce a small amount of stretching-induced crystallization contributing to the orientation increase. In contrast, because molecules in the crystalline structure are more tightly packed than in the amorphous regions, crystallization (mainly induced by the thermal treatment) creates a shrinking force within the fibers. This increases the resistance in the fiber to the applied stress load along the fibers, leading to a tendency for reducing crystal orientation. In other words, chain scission and crystallization are two opposing effects on the crystal orientation. The thermal treatment at 80 °C led to a more significant crystallinity increase in the fiber with DR1.0 and DR1.2 (Fig. 5). During irradiation at 80 °C with 25 kGy, the crystallization effect counteracted the impact of chain scission in these fibers, resulting in no noticeable change in crystal orientation. In the case of fibers with DR1.4 and DR1.6, the increase in crystallinity was less pronounced so that the chain scission effect dominated over the crystallization effect, leading to an increase in crystal orientation. This hypothesis is proved by analyzing the crystal orientation of the fibers with more EB-induced chain scission, which are the fibers irradiated with a high irradiation dose of 250 kGy. The signal intensities of fibers across all four DRs increased after the exposure of the irradiation dose of 250 kGy, compared to their non-irradiated counterparts (0 kGy), as shown in Fig. 9(a)–(d). The 2D patterns of the thermal-treated non-irradiated (80 °C, 0 kGy) and irradiated (80 °C, 250 kGy) fiber with DR 1.6 were also presented for an example in Fig. 9(e) and (f). Moreover, a decrease in diameter in the fibers irradiated with the high dose of 250 kGy can be found, shown in supplementary SFig. 4. This suggests that the enhancement of chain scission increased the crystal orientation and decreased the internal resistance to the stress applied along the fibers (stretching frame setup) making an additional stretching on fibers. This additional stretching leads to the realignment of the pre-existing crystal as well as the stretching-induced crystallization along the fiber as it was illustrated above.

4.2. Investigation of stretching effect – irradiation of PLA with (i.e. fiber) and without (i.e. bulk) oriented amorphous chains

4.2.1. Crystallinity and diameter change of PLA fiber (with oriented amorphous chains)

The industrial commonly-used PLA fibers discussed above have undergone both crystallization and stretching in the melt spinning. To separate the effect of stretching from crystallization, the EB irradiation modification on the amorphous fibers that almost without crystallization was investigated. To produce the amorphous PLA fibers, the low winding velocities (V), which are 50, 75, 100 and 150 m min^{-1}, were applied in melt spinning without a post-drawing process to avoid the formation of drawing-induced crystalline structure. The four types of neat fibers were confirmed have nearly 0 % crystallinities by DSC, indicating they are generally amorphous (see supplementary SFig. 25 for calculation details). On the other hand, the cold crystallization occurred during the elevated temperature irradiation also contributes to the high crystallinity. As it was shown in Fig. 10, the first DSC heating scans of the amorphous fibers revealed a heat flow plateau between the T_g and the onset of cold crystallization, which is different from the result of crystallized PLA fibers discussed in the previous section 4.1. Performing the

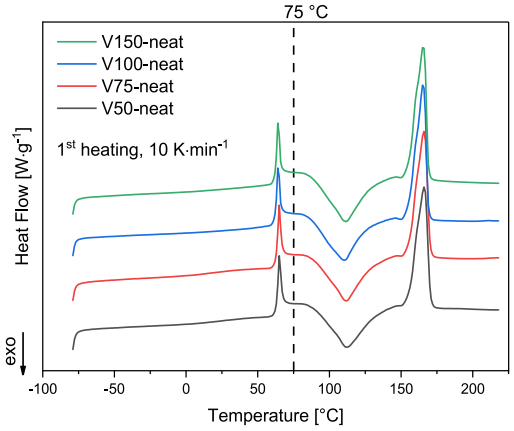

Fig. 10. DSC thermograms (first heating) of neat PLA fibers, which are spun at different winding velocities V (50, 75, 100 and 150 m·min^{-1}).

Table 5
Diameters and fineness of neat (25 °C) and thermally-treated (75 °C) amorphous PLA fibers which are spun at different winding velocities V.

V [m·min^{-1}]	Diameter* [μm]		Fineness [dtex]	
	Neat (25 °C, 0 kGy)	75 °C, 0 kGy	Neat (25 °C, 0 kGy)	75 °C, 0 kGy
50	140 ± 2	119 ± 3	955	869
75	116 ± 2	99 ± 2	629	607
100	103 ± 3	83 ± 2	489	450
150	87 ± 1	67 ± 1	324	299

*Average value ± standard deviation.

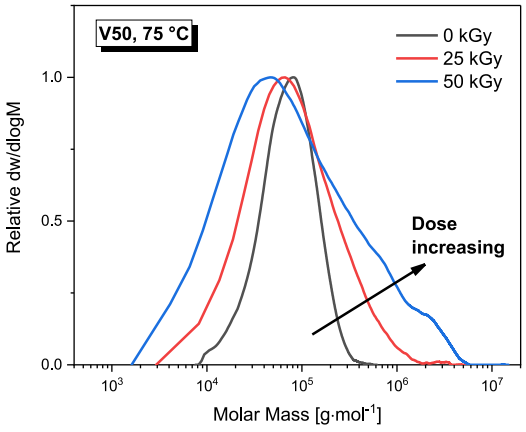

Fig. 11. Relative molar mass distribution of non-irradiated (0 kGy) and irradiated (25 or 50 kGy) amorphous PLA fibers that spun at winding velocities V of 50 m·min^{-1}.

Table 6
M_n, M_w and M_w/M_n of non-irradiated (0 kGy) and irradiated (25 kGy or 50 kGy) amorphous fibers with different winding velocities V.

V [m·min^{-1}]	Irradiation Temperature [°C]	Irradiation Dose [kGy]	M_n* [kg·mol^{-1}]	M_w* [kg·mol^{-1}]	M_w/M_n
50	75	0	55.0 ± 1.8	85.1 ± 1.1	1.5
50	75	25	40.2 ± 1.7	133.7 ± 9.0	3.3
50	75	50	24.8 ± 3.4	246.3 ± 18.5	10.1
75	75	0	57.5 ± 2.0	89.6 ± 1.2	1.6
75	75	25	30.0 ± 2.8	133.7 ± 3.7	4.5
75	75	50	23.6 ± 3.7	225.3 ± 8.6	9.7
100	75	0	56.2 ± 3.9	87.3 ± 1.8	1.6
100	75	25	42.3 ± 3.6	152.6 ± 3.9	3.6
100	75	50	20.2 ± 0.7	196.7 ± 12.0	9.7
150	75	0	55.0 ± 0.5	89.0 ± 1.0	1.6
150	75	25	32.9 ± 1.9	118.8 ± 4.2	3.6
150	75	50	25.6 ± 5.5	249.3 ± 4.3	10.1

*Average value ± standard deviation.

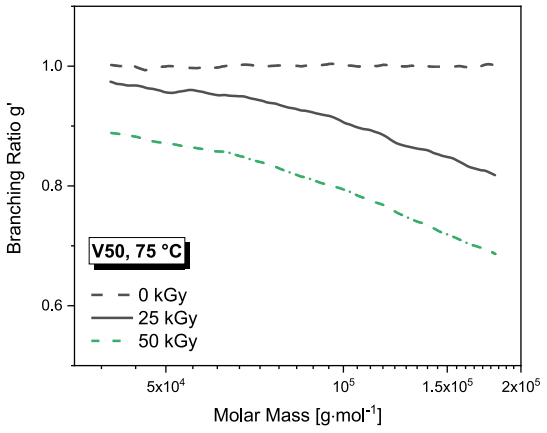

Fig. 12. g' plot of non-irradiated (0 kGy) and irradiated (25 or 50 kGy) amorphous fibers that spun at winding velocities V of 50 m·min^{-1}.

irradiation in the temperature range of the plateau prevents fibers from the cold crystallization while providing sufficient chain mobility for intermolecular backbone radical recombination. Higher temperature can lead to higher chain mobility, thereby the higher temperature is favorable to EB-induced branching. However, based on our heating control device, the temperature cannot be controlled at an exact value in the whole irradiation, the temperature is always fluctuating with an error of ±3 °C. Thus, since the irradiation temperature of 80 °C (used for crystalline PLA fibers in section 4.1) is close to the onset of cold crystallization in amorphous fibers, a slightly lower irradiation temperature of 75 °C was selected for the amorphous fibers. After thermal treatment at 75 °C, the DSC results showed that the treated fibers, labeled as '75 °C, 0 kGy', remained nearly amorphous (calculation details in supplementary SFig. 26). The diameters with fineness of both neat and thermally-treated amorphous fibers were listed in Table 5 (microscope images in supplementary SFigss. 27–28). It was found these amorphous fibers underwent an additional stretching during the irradiation at 75 °C with the stretching frame setup, as the diameters were decreased after thermal treatment, although the shrinkage was prevented. Since no significant increase in crystallinity was observed in the thermally-treated fibers, this additional stretching likely resulted in an additional chain orientation within the amorphous regions. The literature has reported the chain orientation in the amorphous phase can be evaluated by X-ray method in some other kinds of polymers [22,23]. However, no distinct X-ray pattern of amorphous orientation was observed in our case, thereby will not be covered in this study.

4.2.2. Molecular structure alteration of PLA fiber (with oriented amorphous chains)

After amorphous PLA fibers receiving a 25 or 50 kGy irradiation, increases in high molar mass components induced by EB irradiation were observed, as indicated by the relative MMD data obtained from SEC measurements (Fig. 11). The difference is minor among fibers with different winding velocity, thereby only the fiber with the velocity of 50 m·min^{-1} is discussed here, the MMD for the others are shown in supplementary SFig. 29. The curves shown are the averages derived from the measured data, with linear interpolation applied between the minimum and maximum molar mass. The raw data (SFig. 30) and chromatograms (SFigss. 31–42) can be found in supplementary. Additionally, the noticeable increases in M_w and dispersity index M_w/M_n were detected with the increasing irradiation doses (Table 6). Since the irradiation was applied on the bundle that consists of 150 individual fibers, it is challenging to ensure that every single fiber experiences the exact same amount of force when using the fiber stretching frame setup. Therefore, the differences observed among fibers irradiated with the same dose but from different series (V50, V75, V100 and V150) could be attributed to processing-related errors. The branching analysis reveals that the g' value decreases with the increasing molar mass (in the range of $4 \times 10^4 - 1.8 \times 10^5$ g·mol^{-1}) when irradiation was performed at a dose of 25 kGy (Fig. 12), indicating that EB exposure induces branching

Table 7
M_n, M_w and M_w/M_n of non-irradiated (0 kGy) and irradiated (25 or 50 kGy) amorphous non-oriented bulk PLA.

	Irradiation Temperature [°C]	Irradiation Dose [kGy]	M_n* [kg·mol^{-1}]	M_w* [kg·mol^{-1}]	M_w/M_n
Amorphous non-oriented PLA bulk	75	0	60.9 ± 0.6	92.0 ± 0.1	1.5
	75	25	39.7 ± 0.5	100.4 ± 1.6	2.5
	75	50	28.3 ± 2.3	131.4 ± 2.8	4.7

*Average value ± standard deviation.

within PLA fiber. Moreover, the g' values decreased as the irradiation dose increased to 50 kGy, indicating that more branch units were generated by increasing the dose, which mirrors the results observed in crystallized fibers (Fig. 7). This suggests that the more EB-induced branched molecules are the reason of the increasing amount of the higher molar mass components observed in Fig. 11. Furthermore, the g' plot of 50 kGy irradiated amorphous fiber shifts downwards compared to the crystallized fiber, a comparison plot was shown in supplementary SFig. 43. The irradiation temperature applied to amorphous fibers is 5 °C lower than the crystallized fibers. Theoretically, the lower temperature results in lower chain mobility. As a result, radical chains have lower possibility to reach each other to achieve the branching reaction so that should have led less branch unit (higher g'). However, as the result shows, it leads to high branch unit actually. This should be attributed to the elimination of crystalline structures. Different from the radical chains in crystallized areas, the radical chains in amorphous areas are better movable at $T > T_g$ and higher possibility to reach each other and react. The g' values remain nearly identical despite variations in winding velocity, suggesting that winding velocity did not significantly influence the number of branch units when using the irradiation method described in this study, in supplementary SFig. 44. The plot of M_n, M_w and FWHM of MMD plots with the irradiation dose are shown in supplementary SFigss. 45–47.

4.2.3. Comparison between PLA with and without oriented amorphous chains

Furthermore, to separate the effect of stretched (oriented) amorphous chain from non-stretched (non-oriented), the comparison between the EB-irradiated amorphous fiber (with oriented amorphous chains) and amorphous bulk (with non-oriented amorphous chains) was carried out. It was observed that the PLA with oriented amorphous chains (fiber), Table 6, showed a more significant M_w increase after irradiation, compared to the PLA with non-oriented amorphous chains (bulk), Table 7 (chromatograms of non-oriented bulk PLA are provided in supplementary SFigss. 48–50, and the crystallinity determination of the neat PLA bulk was presented in our previous work [20]). Take fiber V50 (Table 6) for an example, the M_w increases for PLA with oriented amorphous chains is from 85.1 kg·mol^{-1} (0 kGy) to 246.3 kg·mol^{-1} after the exposure of 50 kGy, whereas for the bulk with non-oriented amorphous chains is from 92.0 kg·mol^{-1} (0 kGy) to 131.4 kg·mol^{-1}. The increase for PLA with amorphous orientation (fiber) is 189 %, while for the non-oriented bulk is 43 %. According to the previous study, in which

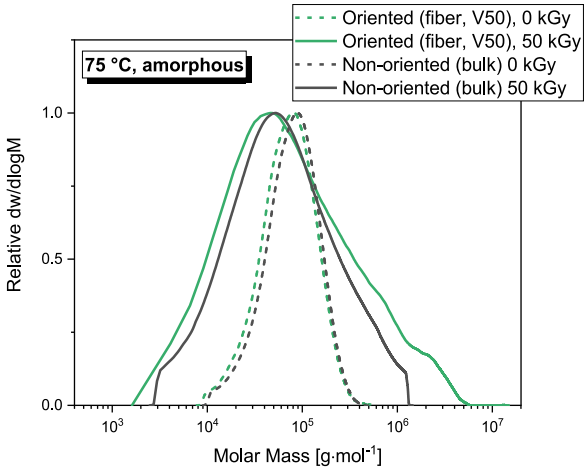

Fig. 13. Comparison of relative molar mass distribution between amorphous PLA fibers (oriented polymer chain system, winding velocity: 50 m·min^{-1}) and non-oriented bulks.

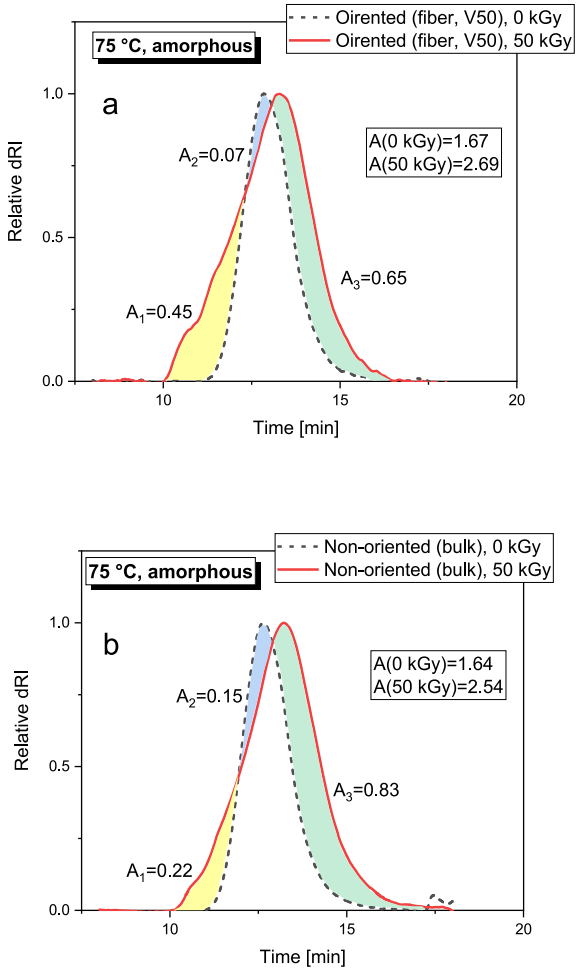

Fig. 14. Relative dRI signal of non-irradiated (0 kGy) and irradiated (50 kGy) amorphous (a) PLA fibers (winding velocity: 50 m·min^{-1}) that with oriented chains and (b) bulks that with non-oriented chains.

irradiations were also performed at the temperature above T_g (i.e. at 80 °C) on amorphous non-oriented PLA bulks, the M_w increase is 102 %, i.e. from 80.6 kg·mol^{-1} (0 kGy) to 162.8 kg·mol^{-1} (50 kGy) [20]. This is another evidence that proves the LCB is enhanced by amorphous chain orientation in fiber shape PLA. A comparison of the relative MMD and relative differential refractive index (dRI) is provided in Figs. 13 and 14, respectively. For the 50 kGy irradiation, the PLA with oriented amorphous chains (fiber V50) has a broader relative MMD and a higher y-axis value in the high molar mass range compared to amorphous non-oriented bulks. The dispersity index of PLA with oriented amorphous chains increases from 1.5 to 10.1, while that of non-oriented bulk increases from 1.5 to 4.7, also indicating the broadening of the MMD. In terms of the dRI signal, the area A_1 is larger for the PLA with oriented amorphous chains (0.45), Fig. 14(a), than for the non-oriented bulk PLA (0.22), Fig. 14(b), and the ratio of area A_1 to the 0 kGy signal area is larger for the PLA with oriented amorphous chains (27 %) than for the non-oriented bulk (13 %). As the shorter elution times in the dRI signal correspond to higher molar mass components, this indicates that the amount of newly generated higher molar mass components in the irradiated PLA with oriented amorphous chains is higher compared to the non-oriented bulk. The ratio of area A_3 to the 0 kGy signal area is 39 % for the PLA with oriented amorphous chains and 51 % for the non-oriented bulk. As A_3 reflects the increase in lower molar mass components, this indicates that the amount of newly generated lower

Table 8
Chain scission $G_{(s)}$ to cross-linking $G_{(x)}$ yield ratio of irradiated amorphous non-oriented bulk PLA, amorphous PLA fibers with different winding velocity (V) 50 – 150 m·min^{-1} and crystallized PLA fibers with draw ratio (DR) 1.0.

Sample Shape	Sample Preparation	Crystallinity of Starting Material	Irradiation Condition	$G_{(s)}/G_{(x)}$
Fiber	V50	~0 %	75 °C, N_2	2.69 (6.24/2.31)
Fiber	V75	~0 %	75 °C, N_2	2.97 (7.64/2.57)
Fiber	V100	~0 %	75 °C, N_2	2.99 (8.01/2.68)
Fiber	V150	~0 %	75 °C, N_2	2.83 (6.42/2.27)
Fiber	DR1.0	~46 %	80 °C, N_2	4.15 (5.31/1.28)
non-oriented bulk	Vacuum compression molding	~0 %	75 °C, N_2	3.27 (5.16/1.58)

molar mass components in the irradiated PLA with oriented amorphous chains is lower compared to the non-oriented bulk case. A possible reason of this phenomenon is the stretching from the fiber winding decreases the distance between molecules, making it easier for radical chains to come closer when the elevated temperature ($T > T_g$) is applied, thus increasing the likelihood of molecular branching during 75 °C irradiation. Moreover, chain disentanglement occurs during stretching-induced chain orientation, which is also favorable to enhance molecular segment mobility for polymer chain at elevated temperature irradiation.

As described in the literature, G value for chain scission (the number of chain scission produced per 100 eV), $G_{(s)}$, and for cross-linking (the number of cross-linking produced per 100 eV), $G_{(x)}$, during low-dose irradiation can be quantified using Equations (3) and (4). These equations derive from measuring the changes in molecular weight of the irradiated polymer, with the units for M_n and M_w in g·mol^{-1} and dose (D) in kGy [37–39]. Based on those equations, the $G_{(s)}/G_{(x)}$ ratio can be expressed by Equation (5), where λ represents the ratio of the slopes from the functions '$1/M_n$ (D kGy) – $1/M_n$ (0 kGy) vs. Dose (D)' to '$1/M_w$ (D kGy) – $1/M_w$ (0 kGy) vs. Dose (D)', Equation (6). The results are shown in Table 8 (with the linear fittings provided in the supplementary SFig. 51). The fitting lines are constrained to pass through the point (0, 0) on the graph for the best fit, as recommended in the literature [40]. By comparing the $G_{(s)}/G_{(x)}$ ratio, the influence of amorphous chain orientation and crystallinity on the dominance of EB-induced reactions during fiber irradiation has been assessed. The results reveal that the amorphous fibers exhibit slightly lower $G_{(s)}/G_{(x)}$ ratios than the amorphous bulk PLA, suggesting that introducing amorphous chain orientation can enhance cross-linking (or LCB). The fiber irradiated at 80 °C from approximately 46 % crystallinity (fiber DR1.0) shows a higher value in $G_{(s)}/G_{(x)}$ ratio compared to amorphous bulk PLA irradiated at 75 °C. This suggests that while chain orientation in the amorphous regions of the fiber can enhance cross-linking (or LCB) during the irradiation above T_g, excessively high crystallinity enhances the dominance of chain scission, even though the crystallized PLA fiber undergoes the irradiation at a temperature that 5 °C higher than the amorphous bulk PLA.

$$\frac{1}{M_n(D\ kGy)} - \frac{1}{M_n(0\ kGy)} = 1.037 \times 10^{-7} \times (G_{(s)} - G_{(x)})D \tag{3}$$

$$\frac{1}{M_w(D\ kGy)} - \frac{1}{M_w(0\ kGy)} = 1.037 \times 10^{-7} \times \frac{1}{2} \times (G_{(s)} - 4G_{(x)})D \tag{4}$$

$$\frac{G_{(s)}}{G_{(x)}} = \frac{2 - 4\lambda}{2 - \lambda} \tag{5}$$

$$\lambda = \frac{G_{(s)} - G_{(x)}}{\frac{1}{2} \times (G_{(s)} - 4G_{(x)})} \tag{6}$$

4.3. Mechanical property of irradiated PLA fibers

Tensile properties were analyzed for the crystallized fibers (produced at high spinning speed with a post-drawing process) and the amorphous fibers (produced at low spinning speed without post-drawing). For all crystallized fibers with different DRs irradiated at 80 °C, the maximum tensile strengths f_H (max), also is the strength at the break point after strain hardening for them, of the thermally treated fibers (80 °C, 0 kGy) were nearly identical to that of their neat counterparts with the same DR (25 °C, 0 kGy), when considering measurement deviations, as shown in Fig. 15(a). Among them, the thermally treated DR1.0, DR1.2 and DR1.4 crystallized fibers showed significant increases in both crystallinity (Fig. 5) and crystal orientation (Fig. 9) than their neat counterparts. However, these changes did not result in a noticeable difference in f_H (max), suggesting that crystallization and increased crystal orientation caused by thermal treatment are not major factors affecting f_H (max). Only DR seems the main influence factor of the resulting tensile properties. Firstly, the newly generated crystalline structures formed in cold crystallization are not the same structures as that formed in spinning and

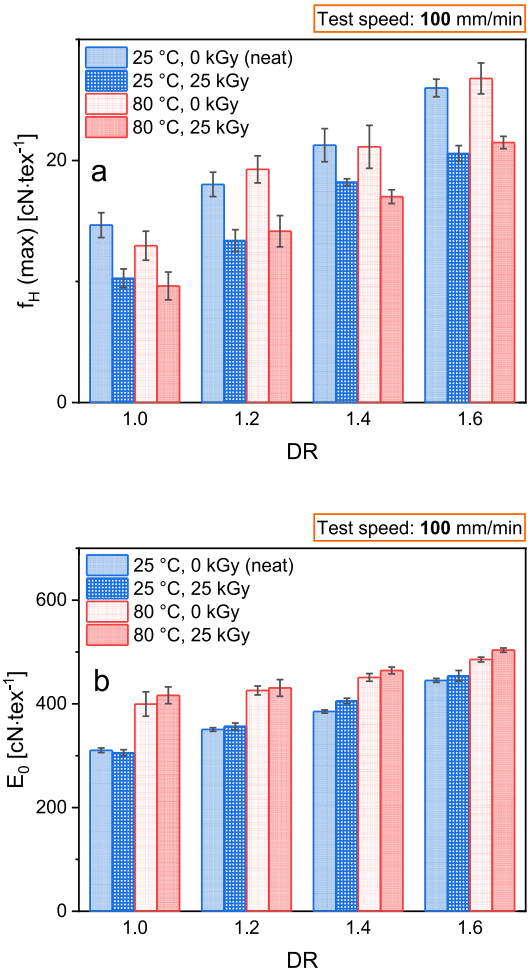

Fig. 15. (a) f_H (max) and (b) E_0 of crystallized fibers with draw ratio DR1.0, 1.2, 1.4 and 1.6 irradiated at 25 °C and 80 °C.

post-drawing process. For instance, the drawing process can increase the content of shish-kebab form. However, although the crystals generated by cold crystallization may form along the fiber direction due to the tension added onto the fiber (stretching frame method), it may be not the shish-kebab form. Moreover, the newly generated crystals seem to include higher content of α′ crystal (less compact crystal) form as it was mentioned in section 4.1.1 (SFig. 1). The difference in crystalline structure morphology and form may play different roles in mechanical property. This could be a reason of the crystallinity is increased by cold crystallization but no obvious change in f_H (max) is found. On the other hand, the semi-crystalline fibers are ductile and break up after a strain hardening. The f_H (max) in this case is the strength at the break-up point. The fiber fracture occurs due to the slippage between chains, the chain pull-out from molecular coils and the breaking of covalent bonds. The breaking up of oriented amorphous chains could be easier than that of chains in crystalline structures. Because in the crystalline structure, chains aligned more compact and are stiff, they will not break-up directly at our tensile test speed. Before they break-up, the crystalline blocks will be separated by stretching force firstly and following by the chains in lamellae are pulled out. Therefore, the maximum tensile strength could depend more on oriented amorphous chains (weak interaction domains), especially the oriented tie molecules which could have more stress concentration, but not on the crystalline structures (strong interaction domains). That is, the key contributor to f_H (max) probably is the chain orientation in the amorphous areas, specifically the alignment of tie-molecules (either inter- or intra-fibril) which is in accordance with findings from other researchers [41]. It seems that the stretching frame setup used in our study effectively maintained the amorphous orientation in the thermally treated fibers with the same DR, leading the f_H (max) to remain unchanged after thermal treatment. This observation also supports the discussion on crystal orientation in section 4.1.3, where the increase in crystal orientation in thermally treated fibers is mainly attributed to the newly formed crystalline structures rather than a change in the original crystal realignment caused by stretching frame setup. The crystals do not distinctly realign indicating there is also no obvious realignment in amorphous areas. It was observed that higher DR resulted in higher f_H (max) for both neat and thermally treated fibers, suggesting that the amorphous orientation is also increased as the DR rose in both cases. On the other hand, 25 kGy-irradiated fibers have lower f_H (max) than their non-irradiated counterparts with the same DR, in the both case of irradiation was performed at 25 °C or 80 °C. This reduction is due to EB-induced chain scission, which leads to an increase in low molar mass components appearing in the fibers (Fig. 6) during these two temperature irradiations. The chain length of the low molecular weight polymer chains is shorter, which results in weaker intermolecular forces (due to less entanglement) than longer chains. As a result, less resistance needs to be overcome for shorter chains during slipping and pull-out from neighboring molecular coils when subjected to tensile force. Once these shorter chains were pull out from the coils, the space they previously occupied becomes vacant, reducing the intermolecular forces between the remaining longer chains. This reduction in intermolecular interaction makes it easier for the longer chains to slip and pull out from the molecular coils under tensile stress. That is, the short chains situated between the long chains play a role of a lubricant. As it was mentioned above, the slippage between chains and the chain pull-out from molecular coils contribute to the fiber break-up, therefore, the EB-induced chain scission resulted in a f_H (max) reduction. When comparing fibers irradiated with 25 kGy at 25 °C to those irradiated with the same dose at 80 °C, their f_H (max) values are nearly identical at the same DR. This could be attributed to the fiber stretching frame setup used during irradiation, which substantially makes the orientation of the amorphous oriented molecules and tie molecules consistently across of them.

As shown in Fig. 15(b), thermally-treated fibers (80 °C) exhibit a higher modulus of elasticity (Young's modulus, E_0) compared to neat fibers (25 °C), irrespective of whether they were irradiated with a dose

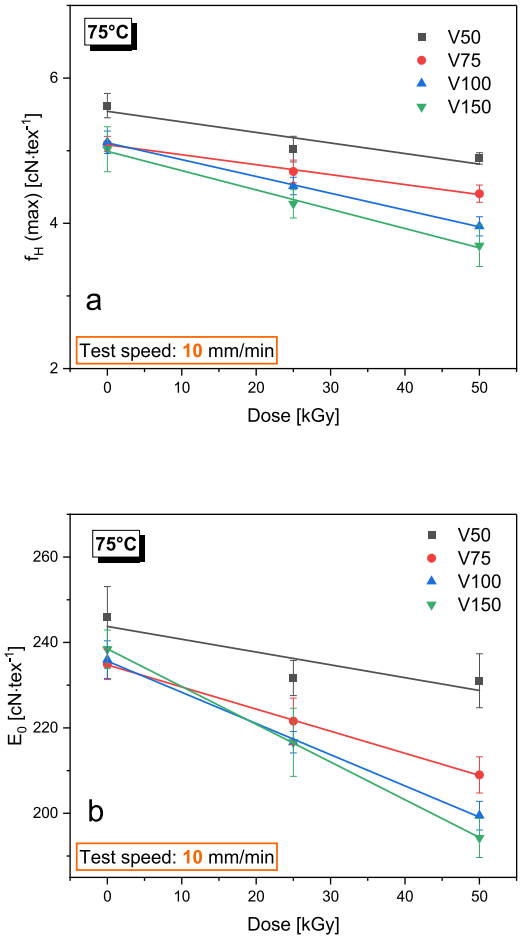

Fig. 16. Dose effect on (a) f_H (max) and (b) E_0 of amorphous PLA fibers with the spinning winding velocity of 50, 75, 100 and 150 m·min^{-1} irradiated at 75 °C.

of 25 kGy or not. This increase is attributed to the formation of crystalline structures in the PLA fibers during the thermal treatment. Furthermore, it reveals that E_0 of thermally-treated fiber rises with increasing DR. Since there are no significant differences in crystallinity and crystal orientation levels among the thermally-treated fibers with the four different DRs, suggesting that E_0 may be not mainly influenced by these factors. The primary distinction between them lies in the orientation of the amorphous regions, which increases with DR. Therefore, it is likely the enhancement of amorphous orientation that contributes to the rise in E_0. Additionally, there is no significant difference in E_0 between non-irradiated fibers (0 kGy) and irradiated fibers (25 kGy) at both 25 °C and 80 °C. This could be attributed to the fact that the crystallinity or the amorphous orientation was not significantly altered by the 25 kGy irradiation dose.

Amorphous fibers normally break very quickly, as they are brittle, when are subjected to a tensile test speed of 100 mm·min^{-1}, which is used for crystallized fibers. In this case, comparison of the mechanical properties between crystallized and amorphous fibers is less meaningful, because the amorphous fibers are obvious more brittle than the crystallized fibers, while to get more information to figure out the dose effect is more meaningful. Therefore, a lower test speed of 10 mm·min^{-1} was employed for amorphous fibers. As shown in Fig. 16(a), the maximum tensile strength f_H (max) of amorphous fibers, which do not have strain hardening, decreases with an increase in the irradiation dose. This

phenomenon is likely due to EB-induced chain scission, similar to that was discussed in the tensile test for crystallized fibers. A slight decrease in f_H (max) was observed for irradiated amorphous fibers as the winding velocity (V, m·min^{-1}) increased. This reduction may be attributed to the fiber stretching frame setup used during irradiation, where a load was applied at the end of the PLA fiber bundle to prevent shrinkage. As indicated by the decrease in diameter shown in Table 5, this method led to additional stretching in the amorphous fibers. The fiber with higher V has more oriented chains in the amorphous areas, leading to higher resistance to the stress force applied along the fiber bundle. As the same load was added to all types of V fibers (section 2.3) during irradiation, fibers with higher V resisted the load more effectively, resulting in less additional stretching, whereas fibers with lower V had less resistance and experienced more stretching due to the applied load. Thus, the applied load made the chains more easily uncoiled and oriented in the amorphous fibers with V50 during irradiation. Accordingly, they gained higher amorphous orientation, resulting in a higher f_H (max). Since the test speed used for amorphous fibers differs from that used for crystallized fibers and mechanical properties depends on the strain rate, directly comparing the results between these two types of fibers would be inappropriate. It is because PLA fibers are the material has viscoelastic characteristic. Therefore, the mechanical property of it are time-dependent [42]. Accordingly, in order to conduct a reliable comparison, the strain-rate should be the same. On the other hand, higher dose resulted in lower E_0 across all four kinds of amorphous PLA fibers (V50, V75, V100 and V150), Fig. 16(b), is likely because of LCB formation disrupting amorphous chain orientation, as the higher irradiation dose also caused more LCB in the fibers as discussed in section 4.2.2.

5. Conclusion

In this study, the EB irradiation effect on PLA fibers modification was investigated without the presence of chemical additives. When the industrial commonly-used fibers were irradiated at a temperature below T_g, the MMD spectra shift a lot towards lower molar mass range, indicating a severe chain scission was induced. It is attributed to the poor chain mobility under that low temperature. In order to improve the chain mobility, an elevated temperature ($T > T_g$) and a novel fiber stretching frame were introduced, in which a permanent constant tension was added along the fiber bundles to prevent fibers from thermal-induced shrinkage. The effect of the tension was discussed based on the characterization of crystal orientation, as the crystal orientation can be seen as an indicator of the tension condition in fibers. The result showed that the irradiation-induced chain scission may decrease the internal resistance force to the tension, resulting in an additional stretching. The main consequences of this study are as follow.

(1) The LCB can be induced in PLA fibers by performing EB irradiation at elevated temperature ($T > T_g$), while a predominant chain scission is induced at the room temperature ($T < T_g$).
(2) The stretching-induced chain orientation in the amorphous domains can improve the EB-induced LCB, which is attributed to the shorter intermolecular distance and the chain disentanglement in the amorphous areas (caused by melt spinning and post-drawing) making the radical chains are easier to reach each other for branching reaction.
(3) The high crystallinity inhibits the EB-induced LCB even the elevated temperature is applied, due to the chains in crystalline region are immobile.
(4) Decreasing the crystallinity enhances the EB-induced LCB in the fiber. The molecule amount of the higher molar mass component and the branch unit are noticeably increased in the amorphous fibers with the increasing irradiation dose. When the irradiation performed with the dose of 50 kGy, more branch units are induced in the amorphous fiber compared to highly crystallized fiber.
(5) The effect of EB-induced chain scission counteracts that of the LCB on the material properties, such as tensile strength, even the irradiation is performed at temperatures above T_g.
(6) Crystal orientation in the fiber increases with higher irradiation dose above T_g. This orientation change is probable because of the interplay between chain scission and cold crystallization. The resulting tensile properties are primarily influenced by the DR and seem to be barely influenced by crystal orientation.

Accordingly, in order to overcome the negative effect of the high crystallinity with enhancing the positive effect of the amorphous chains orientation, introduce the EB into the stretching-oriented melt during the melt spinning process is a sensible solution.

CRediT authorship contribution statement

Yinglan Zhang: Writing – review & editing, Writing – original draft, Methodology, Investigation. **Michael Thomas Müller:** Writing – review & editing, Supervision, Methodology, Investigation, Conceptualization. **Regine Boldt:** Writing – review & editing, Investigation. **Albena Lederer:** Writing – review & editing, Investigation. **Matthias Schwartzkopf:** Data curation, Formal analysis, Writing – review & editing. **Norbert Smolka:** Writing – review & editing, Investigation. **Markus Stommel:** Writing – review & editing, Supervision.

Declaration of competing interest

We declare that we have no known competing financial interests or personal relationships that could have appeared to influence the work reported in this paper.

Acknowledgement

Thanks to Dr. Susanne Boye and Alissa Seifert (SEC); Karl Tuisl and Carsten Zschech (EB irradiation); Anne-Katrin Leopold (the fiber stretching frame setup is based on her work), Sabine Krause (DSC of crystallized fibers), Maria Auf der Landwehr (SEM) and Jacqueline Böhme (diameter and sol-gel extraction of fibers) for measurements, Dr. Harald Brünig, Mathias Häschel for melt spinning (all from Leibniz-Institut für Polymerforschung Dresden e.V.).

Appendix A. Supplementary data

Supplementary data to this article can be found online at https://doi.org/10.1016/j.polymer.2025.128567.

Data availability

Data will be made available on request.

References

[1] J. Feng, Preparation and properties of poly(lactic acid) melt spun fiber aligned and disordered scaffolds, Mater. Lett. 192 (2017) 153–156.
[2] K.M.Z. Hossain, et al., Tubular scaffold with shape recovery effect for cell guide applications, J. Funct. Biomater. 6 (2015) 564–584, https://doi.org/10.3390/jfb6030564.
[3] N. Behary, et al., Nano-structured ridged micro-filaments (≥100 μm diameter) produced using a single step strategy for improved bone cell adhesion and proliferation in textile scaffolds, Molecules 27 (2022) 3790.
[4] J. Hahn, et al., Viscoelastic behavior of embroidered scaffolds for ACL tissue engineering made of PLA and P(LA-CL) after in vitro degradation, Int. J. Mol. Sci. 20 (2019), https://doi.org/10.3390/ijms20184655.
[5] J. Hahn, et al., Long-term hydrolytic degradation study on polymer-based embroidered scaffolds for ligament tissue engineering, J. Ind. Textil. 47 (6) (2017) 1305–1320.
[6] J. Gu, et al., Functionalization of biodegradable PLA nonwoven fabric as superoleophilic and superhydrophobic material for efficient oil absorption and oil/water separation, ACS Appl. Mater. Interfaces 9 (7) (2017) 5968–5973.

[7] B.Y. Shin, D.H. Han, R. Narayan, Rheological and thermal properties of the PLA modified by electron beam irradiation in the presence of functional monomer, J. Polym. Environ. 18 (4) (2010) 558–566.
[8] M. Bednarek, K. Borska, P. Kubisa, Crosslinking of polylactide by high energy irradiation and photo-curing, Molecules 25 (21) (2020) 4919.
[9] E.C. Grosvenor, et al., On the mechanism of electron beam radiation-induced modification of poly(lactic acid) for applications in biodegradable food packaging, Appl. Sci. 12 (4) (2022) 1819.
[10] M. Kodal, A.A. Wis, G. Ozkoc, The mechanical, thermal and morphological properties of γ-irradiated PLA/TAIC and PLA/OvPOSS, Radiat. Phys. Chem. 153 (2018) 214–225.
[11] N. Nagasawa, et al., Radiation-induced crosslinking and post-processing of poly(l-lactic acid) composite, Radiat. Phys. Chem. 80 (2) (2011) 145–148.
[12] T.M. Quynh, et al., Properties of crosslinked polylactides (PLLA & PDLA) by radiation and its biodegradability, Eur. Polym. J. 43 (5) (2007) 1779–1785.
[13] M. Vidotto, et al., Effects of γ-radiation on structure and properties of poly(lactic acid) filaments, Radiat. Phys. Chem. 184 (2021) 109456.
[14] K.-L.G. Ho, A.L. Pometto Iii, Effects of electron-beam irradiation and ultraviolet light (365 nm) on polylactic acid plastic films, J. Environ. Polym. Degrad. 7 (2) (1999) 93–100.
[15] C. Birkinshaw, et al., Irradiation of poly-d,l-lactide, Polym. Degrad. Stabil. 38 (3) (1992) 249–253.
[16] P. Rytlewski, et al., Influence of some crosslinking agents on thermal and mechanical properties of electron beam irradiated polylactide, Radiat. Phys. Chem. 79 (10) (2010) 1052–1057.
[17] H. Fang, et al., Bimodal architecture and rheological and foaming properties for gamma-irradiated long-chain branched polylactides, RSC Adv. 3 (23) (2013) 8783–8795.
[18] N. Nagasawa, et al., Application of poly(lactic acid) modified by radiation crosslinking, Nucl. Instrum. Methods Phys. Res. Sect. B Beam Interact. Mater. Atoms 236 (1) (2005) 611–616.
[19] Y. Huang, et al., Electron beam treatment of polylactide at elevated temperature in nitrogen atmosphere, Radiat. Phys. Chem. 159 (2019) 166–173.
[20] Y. Zhang, et al., Crystallinity effect on electron-induced molecular structure transformations in additive-free PLA, Polymer 265 (2023) 125609.
[21] T. Aouat, et al., The effect of gamma-irradiation on morphology and properties of melt-spun poly (lactic acid)/cellulose fibers, Polym. Degrad. Stabil. 160 (2019) 14–23.
[22] E. Perret, R. Hufenus, Insights into strain-induced solid mesophases in melt-spun polymer fibers, Polymer 229 (2021) 124010.
[23] E. Perret, R. Hufenus, Fitting of 2D WAXD data: mesophases in polymer fibers, Data Brief 39 (2021) 107466.
[24] J.D. Menczel, M. Jaffe, 5 - thermomechanical analysis of fibers, in: M. Jaffe, J. D. Menczel (Eds.), Thermal Analysis of Textiles and Fibers, Woodhead Publishing, 2020, pp. 81–94.
[25] Enhancement of Radiation Crosslinking, in: Radiation Processing of Polymer Materials and its Industrial Applications, 2012, pp. 71–102.
[26] T. Sasuga, M, Takehisa, Effect of high pressure on radiation-induced cross-linking of synthetic rubbers, J. Macromol. Sci. B 11 (3) (1975) 389–401.
[27] J.D. Menczel, W.S. Kohl, 3 - differential scanning calorimetry (DSC) in fiber research, in: M. Jaffe, J.D. Menczel (Eds.), Thermal Analysis of Textiles and Fibers, Woodhead Publishing, 2020, pp. 17–69.
[28] N.P. Tipnis, D.J. Burgess, Sterilization of implantable polymer-based medical devices: a review, Int. J. Pharm. 544 (2) (2018) 455–460.
[29] H.-M. Ng, et al., Effect of electron beam irradiation sterilization on biomedical polylactic acid composite filled with scomberomorus Guttatus-derived hydroxyapatite, Compos. B Eng. 176 (2019) 107273.
[30] D. Garlotta, A literature review of Poly(Lactic acid), J. Polym. Environ. 9 (2) (2001) 63–84.
[31] A. Buffet, et al., P03, the microfocus and nanofocus X-ray scattering (MiNaXS) beamline of the PETRA III storage ring: the microfocus endstation, J. Synchrotron Radiat. 19 (Pt 4) (2012) 647–653.
[32] B.H. Zimm, W.H. Stockmayer, The dimensions of chain molecules containing branches and rings, J. Chem. Phys. 17 (12) (1949) 1301–1314.
[33] P.J. Flory, T.G. Fox, Treatment of intrinsic viscosities, J. Am. Chem. Soc. 73 (5) (1951) 1904–1908.
[34] R. Dockhorn, et al., Polyolefins formed by chain walking catalysis—A matter of branching density only? J. Am. Chem. Soc. 141 (39) (2019) 15586–15596.
[35] J. Engelke, et al., An in-depth analysis approach enabling precision single chain nanoparticle design, Polym. Chem. 11 (41) (2020) 6559–6578.
[36] L. Plüschke, et al., Fractionation of chain walking polyethylene and elucidation of branching, conformation and molar mass distributions, Int. J. Polym. Anal. Char. 26 (1) (2021) 47–59.
[37] J.H. O'Donnell, Chemistry of radiation degradation of polymers, in: Radiation Effects on Polymers, American Chemical Society, 1991, pp. 402–413.
[38] Fundamentals of Radiation Crosslinking, in: Radiation Processing of Polymer Materials and Its Industrial Applications, 2012, pp. 26–70.
[39] C.L. Moad, D.J. Winzor, Quantitative characterization of radiation degradation in polymers by evaluation of scission and cross-linking yields, Prog. Polym. Sci. 23 (5) (1998) 759–813.
[40] D.J.T. Hill, et al., Molecular weight changes and scission and crosslinking in poly (dimethyl siloxane) on gamma radiolysis, Radiat. Phys. Chem. 62 (1) (2001) 11–17.
[41] R. Kotek, et al., 7 - production of polyolefins, in: S.C.O. Ugbolue (Ed.), Polyolefin Fibres, second ed., Woodhead Publishing, 2017, pp. 189–264.
[42] M. Balasubramanian, R. Saravanan, V. Shanmugam, Impact of strain rate on mechanical properties of polylatic acid fabricated by fusion deposition modeling, Polym. Adv. Technol. 35 (3) (2024) e6335.
[43] Y. Zhang, et al., Electron-induced alteration of PLA chain structure, ACS Appl. Polym. Mater. 6 (1) (2024) 419–432.